Cell. Mol. Life Sci. 63 (2006) 2162–2174
1420-682X/06/182162-13
DOI 10.1007/s00018-006-6200-x

Cellular and Molecular Life Sciences

Research Article

Molecular characterization of the tumor-associated antigen AAA-TOB3

M. Schaffrik, B. Mack, C. Matthias, J. Rauch and O. Gires*

Clinical Cooperation Group Molecular Oncology, Department of Head and Neck Research, Ludwig-Maximilians University Munich and GSF-National Research Center for Environment and Health, Marchioninistr. 15, 81377 Munich (Germany), Fax: +49 89 70956896, e-mail: olivier.gires@med.uni-muenchen.de

Received 2 May 2006; received after revision 22 June 2006; accepted 29 June 2006
Online First 11 August 2006

Abstract. In search for new valuable tumor-associated antigens using the AMIDA technique, we identified the KIAA1273-AAA-TOB3 protein. KIAA1273 and AAA-TOB3 were considered synonyms for the *atad3B* gene product. We show that the *atad3b* gene encodes two distinct proteins, both overexpressed in head and neck carcinomas and required for correct cell division. Both products differ within the N terminus, are generated upon distinct transcription initiation sites, and have been termed AAA-TOB3$_s$ and AAA-TOB3$_l$. Both isoforms are early targets of c-myc and are located in mitochondria. A previous report suggested pro-apoptotic properties of the murine homolog of AAA-TOB3$_l$. Here, we did not observe any pro-apoptotic effects in human cell lines, overexpressing h-AAA-TOB3$_s$ or h-AAA-TOB3$_l$. By contrast, the specific knock-down of both mRNAs resulted in polynuclear cells and decreased proliferation, along with dysfunctional cell division followed by increased apoptosis. Thus, the present data suggest a role for AAA-TOB3$_{s/l}$ in tumor progression.

Keywords. AAA-TOB3, KIAA1273, AMIDA, mitochondrial protein, apoptosis.

Introduction

AMIDA, the antibody-mediated identification of antigens, is a proteomics-based technology designed to isolate potential tumor-associated antigens (TAAs) based on the humoral response they elicit *in vivo* [1, 2]. We have reported on the identification of the KIAA1273/AAA-TOB3 protein in head and neck squamous cell carcinomas, using an autologous version of AMIDA [1]. KIAA1273 and AAA-TOB3 were regarded as synonyms for the same protein product of the *atad3b* gene locus (ATPase family AAA domain containing protein 3B). For the sake of simplicity, the term AAA-TOB3 will be used in the present report. Sequence homology assigned AAA-TOB3 to the large family of ATPases associated with various cellular activities (AAA-ATPase), including proteins important for proteolysis, membrane fusion, DNA replication or intracellular trafficking [3–6]. The function and localization of human AAA-TOB3 is poorly studied so far. *In situ* hybridization experiments revealed the expression of AAA-TOB3 mRNA in the cells of the basal membrane layer of healthy squamous epithelium, whereas suprabasal layers did not express the mRNA [1]. Unpublished results from Pillai et al. have shown that human AAA-TOB3 facilitated protein transport from the endoplasmic reticulum to the Golgi apparatus (http://mghra.partners.org/narratives/PillaiS.htm). Furthermore, the murine homolog of AAA-TOB3, mAAA-TOB3, has been isolated in a screening for proteins of the inner mitochondrial membrane [7]. When transferred into human carcinoma cells, mAAA-TOB3 induced apoptosis, which was counteracted upon treatment of the cells with the apoptosis inhibitor ZVAD. Similar findings for other proteins that are overexpressed

* Corresponding author.

in tumors and have pro-apoptotic potential have been reported. For example, cleaved variants of the MAGE-A4 tumor-associated cancer-testis antigen induced p53-dependent and -independent apoptosis [8]. Comparable results were described for the preferentially expressed antigen of melanomas PRAME [9]. Thus, the elucidation of the open question whether human TOB3 is also pro-apoptotic appeared of major importance.

Further confusion arose from recent BLASTn searches with the AAA-TOB3 sequence. The alignment of AAA-TOB3 on the human transcriptome yielded an additional open reading frame assigned to the *atad3b* gene locus, which substantially differs in the 5′ region. This prompted us to analyze in a more detailed fashion the products of the *atad3b* gene locus in carcinoma cells. Here we demonstrate the existence of two isoforms of the AAA-TOB3 protein, AAA-TOB3$_l$ and AAA-TOB3$_s$, which differ in length and are generated upon differential transcription initiation start usage. Detailed analysis revealed the overexpression of both isoforms in head and neck squamous cell carcinomas and their mitochondrial localization. In contrast to their murine counterpart [7], neither AAA-TOB3$_s$ nor AAA-TOB3$_l$ was pro-apoptotic. However, the knock-down of both proteins using specific small interfering RNAs (siRNAs) resulted in a decreased proliferation and the appearance of polynuclear cells along with dysfunctional cell division. Subsequently, cells displayed an increased cell size, vacuolization, granularity, and ultimately died by apoptosis. Thus, AAA-TOB3$_s$ and AAA-TOB3$_l$ are two distinct proteins expressed from a single gene locus, which functionally feed into the process of cell division, and are overexpressed in carcinomas.

Materials and methods

Cell lines and flow cytometry. GHD-1 cells were established from a biopsy of a hypopharynx carcinoma patient [10]. ANT-1, FaDu, PCI1, PCI13, and 22A are head and neck squamous cell carinoma lines. HeLa is a cervix cell line (ATCC CCL-2). All cell lines were cultured in standard DMEM supplemented with 10% fetal calf serum (FCS). For flow cytometry analysis, cells were washed twice in PBS and resuspended in PBS supplemented with 3% FCS. Cell size, granularity, and fluorescences were assessed in a FACSCalibur device (BD Clontech, Heidelberg, Germany).

***In-situ* hybridization.** *In situ* hybridization was performed as described elsewhere [1].

Laser scanning fluorescence microscopy. HeLa and GHD-1 cells expressing YFP-fusion proteins were stained with MitoTracker Red™ (Molecular Probes, Eugene, OR, USA) and living cells analyzed in a fluorescence laser scanning system (TCS-SP2 scanning system and DM IRB inverted microscope; Leica, Solms, Germany).

Immunohistochemistry. For immunohistochemistry, 1×10^4 cells/well were grown for 12–18 h in eight-well chamber slides (Nunc, Wiesbaden, Germany). Cells were then transiently transfected with expression plasmids for hemagglutinin (HA)-tagged AAA-TOB3$_{s/l}$ and incubated for a further 20 h. They were then fixed and permeabilized (acetone, 10 min, room temperature), before detection with an HA-specific monoclonal antibody (1:100, Roche, Mannheim, Germany) in combination with a biotinylated secondary antibody and avidin-biotin-peroxidase complex. Finally, cells were stained with amino-ethyl-carcazole (AEC) and mounted using Kaisers glycerin gelatin (Merck, Darmstadt, Germany). Transfected cells were viewed on an inverted microscope (Axiovert 200; Zeiss) at 400-fold magnification, and images were captured using a digital camera (Hamamatsu Photonics, Hersching).

Cell viability and annexin-V staining. GHD-1 and HeLa cells were plated at a density of 4000 cells/well in 96-well plates and allowed to grow for 24 h before treatment. Cells were then transfected with 50 ng or 100 ng target DNA, using MATRA (IBA, Göttingen, Germany). Transfection efficiency was 70% and 55% in average for GHD-1 and HeLa cells, respectively. For MTT assays, cells were transfected with increasing amounts of AAA-TOB3$_s$ and AAA-TOB3$_l$ expression plasmid (*add* 50 or 100 ng carrier-DNA, respectively). Cell viability was evaluated 24 and 48 h after transfection. For annexin-V and propidium iodide (PI) stainings, adherent cells were transfected with YFP fusion constructs, washed 48 h later with PBS, and stained with annexin-V Biotin labeling kit according to the manufacturer's protocol (Roche, Mannheim, Germany). Annexin-V was visualized using Alexa 594-conjugated streptavidin (Molecular Probes). Nuclei were visualized with Hoechst 33342. AAA-TOB3$_s$-YFP, AAA-TOB3$_l$-YFP, annexin-V, and PI-positive cells were related to the entirety of transfected cells.

Time-lapse microscopy. GHD-1 cells were grown on glass plates and transfected 24 h after plating. Time-lapse experiments were started 4 h after transfection. Cells were kept at 37 °C during microscopic observation. Digital images were acquired as a time-lapse series using a Zeiss Axiovert 200-M microscope equipped with a Hamamatsu 4747-95 digital CCD camera and the Improvision openLab Software. Each series contained ~700 images taken at 5-min interval. Images were prepared for presentation with the Adobe Photoshop software.

Laser-capture microdissection. Tissue cryosections (healthy mucosa and HNSCC, $n = 4$ each) were processed in serial 10-µm sections, mounted on superfrost plus slides (Menzel, Braunschweig, Germany). Thereafter, slides were immediately immersed in ice-cold acetone (60 s), air dried (60 s), stained with filtered Meyers hematoxylin (30 s), and air-dried for further 5 min. All steps were performed under RNase-free conditions. LCM was performed with a CellCut system® (Molecular Machines & Industries, Eching, Germany) using a 355-nm laser beam at an average output power of 4 mW. Cells in the tumor areas and healthy epithelium were readily identified and captured; tumor cells adjacent to necrotic areas or cells with a small regular nucleus, endothelial cells, and blood cells were avoided. The isolated samples are trapped using the MMI Isolation Cap®. Total RNA was isolated from the LCM-collected samples using the MicroRNA isolation kit (Qiagen, Hilden, Germany) according to manufacturer's protocol. The RNA pellet was redissolved in water treated with sterile diethylpyrocarbonate. Reverse transcription was performed as described below.

Real-time PCR. Real-time PCR was performed in a Light-Cycler® device (Roche, Mannheim, Germany) in a reaction volume of 10 µl with 1 µM of each primer, 2 mM $MgCl_2$, 10 ng cDNA, and SYBR Green I (LC-FastStart DNA Master, Roche) according to the manufacturer's protocol. The following primer pairs were used: CD19, 5′-CTCCTTCTCCAACGCTGAGT-3′ and 5′-TGGAAGTGTCACTGGCATGT-3′; AAA-$TOB3_s$, 5′-CTGGTGAGTGCTGTGCTCTGCAG-3′ and 5′-GTTGCTGCTGCTTCAGTTGGTC-3′; AAA-$TOB3_l$, 5′-GTTGGAGCAACAGCAAGCTCAAA-3′ and 5′-GTTGCTGCTGCTTCAGTTGGTC-3′; c-myc, 5′-TCCGTCCTCGGATTCTCTGC-3′ and 5′-CCAGTGGGCTGTGAGGAGGT-3′; β-actin, 5′-ACACTGTGCCCATCTACGAGG-3′ and 5′-AGGGGCCGGACTCGTCATACT-3′. Cycling conditions were: 1 cycle of 95 °C for 10 min, and 45 cycles of 95 °C for 1 s, 68–70 °C for 10 s, and 72 °C for 5–25 s.

RNA Isolation from cell lines. Total RNA was isolated from the cell lines HeLa and GHD-1 with the peqGOLD TriFast kit (PeqLab, Erlangen, Germany).

5′-RACE and RT-PCR. Adapter-linked full-length cDNA was synthesized according to the manufacturer's protocol (Gene Racer™ Kit, Invitrogen, Karlsruhe, Germany). Reverse transcription of the RNA was performed using Superscript II (Invitrogen). The 5′-RACE and the PCR reactions were carried out using Advantage GC2 polymerase mix (BD Clontech) as follows: 95 °C for 3 min; then 5 cycles of 95 °C for 20 s and 68 °C for 60 s; then 35 cycles of 95 °C for 20 s, 65 °C for 30 s, 68 °C for 60 s and 68 °C for 5 min (primer 1: 5′-TTGGACAGAGTGTCACTCTGT-3′, primer 2: 5′-GTTCAACCTCCTGCCTCAGC-3′, primer 3: 5′-GCCTGCCACCACATCTGGC-3′, primer 4: 5′-AGGGGGTTCACATGTTGTCCAG-3′, primer 5: 5′-ATGCAGCTGGAAGCCCTGAACC-3′, primer 6: 5′-CGCGGCCAATCAAGGGCT-3′, primer 7: 5′-CCTGCGCAGTGGTCCTGGGCCA-3′, primer 8: 5′-GTGGAGGCTGCTCCCAGCCGCG-3′, primer 9: 5′-ATGTCGTGGCTCTTCGGCGTTAA-3′, primer A: 5′-CTGCAGAGCACCACTCACCAG-3′, primer B: 5′-CACCACGCTCAGGGTCTTCCTCC-3′). The 5′-RACE products were cloned in pDrive (Qiagen) prior to sequencing.

DNA cloning. All the constructs in this study were generated by standard PCR cloning procedures using RZPD full open reading frame clones IRALp962O1117 (AAA-$TOB3_s$) and IRALp962D034Q2 (AAA-$TOB3_l$). The amplified sequences were C-terminally fused to the HA epitope (YPYDVPDYA) by PCR and cloned in 141pCAG-3SIP vector (kindly gift of Dr. T. Schröder, GSF, Munich, Germany) or cloned into the pEYFP-N1 vector (BD Clontech, Hilden, Germany) to generate C-terminal YFP-fusion proteins. All constructs were sequenced to verify the fidelity of the cDNA sequences obtained.

SiRNA. Cells (5×10^5 cells/well) were plated in 6-well plates and allowed to grow for 24 h before transfection with 100 nM target-specific siRNA and control siRNA using MATRA transfection reagent. At 2 h post transfection, cells were trypsinized and plated into cell culture plate (diameter 10 cm). Cells were counted at 24, 48, 72 and 96 h post transfection. At 72 h after transfection, cells were viewed on an inverted microscope (Axiovert 200; Zeiss, Oberkochen, Germany) at a 400-fold magnification, images were captured using a digital camera (Hamamatsu, Hersching, Germany), and analyzed by flow cytometry. The following siRNA sequences were used: control, 5′-UUAACCCGAUGAAUUCUUCTT-3′; AAA-$TOB3_{s/l}$, 5′-AGACGCUGUUUGCCAAGAA-3′.

AAA-$TOB3_s$ and AAA-$TOB3_l$ antibodies. To generate rabbit polyclonal antisera directed against AAA-$TOB3_s$- and AAA-$TOB3_l$-specific peptides, RGLGDRPAPK-DKWSN (AAA-$TOB3_l$) and CRAGAVQTQERLSGS (AAA-$TOB3_s$), were used to immunize rabbits (Biogenes, Berlin, Germany).

Results

A current search of homologies for AAA-TOB3 using the BLASTn algorithm yielded expected sequences, but also two additional expressed short sequence tags (ESTs gene bank accession BC009938 and AB033099), which

substantially differ in the 5′-region. Accordingly, the predicted protein sequences resulting from both AAA-TOB3 mRNAs shared the C-terminal region, but no homology in the N termini. Based on the difference in length, we termed these two potential isoforms AAA-$TOB3_s$ (small) and AAA-$TOB3_l$ (large). Amino acid 1–52 from AAA-$TOB3_s$ and 1–94 from AAA-$TOB3_l$ are different with the exception of two leucine residues at amino acid position 13 and 51, and one alanine residue at position 19 of AAA-$TOB3_s$ (Fig. 1a, b). AAA-$TOB3_l$ is composed of 16 exons encoded by the *atad3b* gene locus. The analysis of the genomic structure revealed the presence of an alternative ATG within intron 2 of AAA-$TOB3_l$, thus suggesting the existence of a second open reading frame. This alternative ATG is in frame with the coding sequence of exon 3 and potentially gives rise to the AAA-$TOB3_s$ mRNA (Fig. 1c). We performed RT-PCRs specific for the differential open reading frames to assess the existence of the assumed AAA-$TOB3_s$ and AAA-$TOB3_l$ mRNA products. Both mRNAs were detectable in head and neck, and cervix carcinoma cell lines (Fig. 1d, upper panel).

To demonstrate the existence of both proteins, specific polyclonal antibodies were generated with peptides covering the respective N terminus. For a control, both proteins were fused to an HA epitope and transiently transfected into GHD-1 (HNSCC) and HeLa (cervical carcinoma) cells. Protein expression was analyzed in wild-type cells and following transient transfection of either the empty vector control or the respective expression vector for AAA-$TOB3_s$-HA or AAA-$TOB3_l$-HA variants. The detection of endogenous and HA-variants of AAA-$TOB3_s$ and AAA-$TOB3_l$ was performed with HA-, AAA-$TOB3_s$-, and AAA-$TOB3_l$-specific antibodies, respectively. Both, AAA-$TOB3_s$ and AAA-$TOB3_l$ were expressed in GHD-1 and HeLa cells (Fig. 1d, lower panel). Expectedly, HA-tagged variants of both proteins were only detectable following exogenous expression, displayed a slight increase in molecular weight due to the additional tag, and were expressed to levels similar to endogenous TOB3 proteins. Thus, AAA-$TOB3_s$ and AAA-$TOB3_l$ are two distinct protein isoforms of the *atad3b* gene locus.

Unfortunately, polyclonal antibodies specific for each protein were not suitable for immunohistochemistry. Hence, we assessed the expression of AAA-$TOB3_s$ and AAA-$TOB3_l$ mRNA as a surrogate. Laser capture microdissection was performed on primary healthy oral mucosa ($n = 4$) and corresponding head and neck carcinomas ($n = 4$), as exemplified in Figure 1e, upper panel. The quantification of each mRNA species was conducted upon real-time PCR with primers specific for the 5′ regions of AAA-$TOB3_s$ and AAA-$TOB3_l$ and normalized for β-actin levels. Three out of four carcinomas tested showed significantly increased expression of AAA-$TOB3_s$ and AAA-$TOB3_l$ mRNA as compared with healthy epithelium of the cognate localization. The overexpression levels of AAA-$TOB3_s$ and AAA-$TOB3_l$ ranged from 5- to 12-fold and 7.2- to 16-fold, respectively (Fig. 1e, lower panel). In the same specimens, the AAA-$TOB3_{s/l}$ mRNA levels were additionally visualized by *in situ* hybridization, confirming the strong overexpression of AAA-$TOB3_{s/l}$ in HNSCCs ($n = 5$) as compared with healthy mucosa of the corresponding area ($n = 5$) (Table 1). Thus, AAA-$TOB3_s$ as well as AAA-$TOB3_l$ mRNAs were overexpressed in head and neck squamous cell carcinomas.

Different mRNAs can be generated upon alternative splicing of the common pre-mRNA or due to a distinct transcription initiation start (TIS) usage. To test these eventualities and to define 5′-untranslated region (UTR) of the isoforms, we performed a full-length 5′-cloning of both mRNAs. Five independent TISs were cloned and sequenced for the AAA-$TOB3_s$ mRNA (Fig. 2a). In addition to TISs described in the literature, one novel initiation site was cloned for the AAA-$TOB3_l$ mRNA (Fig. 2b). The alignment of the cloned 5′-UTRs of AAA-$TOB3_s$ and AAA-$TOB3_l$ showed no homology whatsoever, thus demonstrating a selective TIS usage and suggesting different promoters for the two mRNAs. The existence of all sequences was confirmed by RT-PCR in two independent cell lines, *i.e.* GHD-1 and HeLa, with primers scanning the cloned 5′-UTRs (Fig. 2a, b). The presence of one additional TIS of AAA-$TOB3_s$, which was not cloned in our approach, was demonstrated as an RT-PCR product generated with a forward primer located in the 5′ region of the first TIS in both cell lines tested (Fig. 2a, primer 2). However, AAA-$TOB3_s$ and AAA-$TOB3_l$ are two different mRNAs generated upon alternative TIS usage within the *atad3b* gene locus.

The *atad3b* gene contains a canonical E-box sequence within intron 1 for the binding of the oncogenic transcription factor c-Myc. This finding prompted us to analyze the expression of AAA-$TOB3_s$ and AAA-$TOB3_l$ in P493-6 cells harboring a conditional *c-myc* allele. In P493-6 B cells, the *c-myc* gene is under the control of a tetracycline-regulated promoter (tet-off) [11]. P493-6 cells were grown in the presence of tetracycline over a time period of 4 days to down-regulate c-Myc expression. The expression of c-Myc, AAA-$TOB3_s$, and AAA-$TOB3_l$ mRNAs was determined afterwards by real-time PCR with specific primers and normalized for CD19 mRNA levels. Upon addition of tetracycline the expression of c-Myc mRNA was reduced to background levels already after 24 h (93% reduction) and remained low throughout the time period of tetracycline addition. AAA-$TOB3_s$ and AAA-$TOB3_l$ mRNA expression was repressed in the same time span by 87% and 92%, respectively (Fig. 2c, upper panel). Noteworthy, the down-regulation of AAA-$TOB3_s$ and AAA-$TOB3_l$ followed the repression of c-Myc with an estimated delay of 2 h. Subsequently, tetracycline

was withdrawn from the culture medium and the re-induction of c-Myc expression was monitored in a kinetic ranging from 0 to 12 h. C-Myc mRNA and protein levels were rapidly up-regulated starting 1 h following tetracycline withdrawal and mRNA expression was induced by a factor of 21 after 12 h (Fig. 2d, and data not shown). Congruently, AAA-TOB3$_s$ and AAA-TOB3$_l$ mRNAs were up-regulated by a factor of 34 and 92 after 12 h, respectively. The regulation of both AAA-TOB3 isoforms perfectly coincided with c-Myc re-induction, with a delay of approximately 1 h.

Next, we analyzed the localization of AAA-TOB3$_s$ and AAA-TOB3$_l$ in human carcinoma cells. Both proteins have predicted transmembrane domains and an AAA-ATPase domain (see Fig. 1b). To assess their localization, both molecules were C-terminally fused with the yellow fluorescent protein (YFP) to generate AAA-TOB3$_s$-YFP and AAA-TOB3$_l$-YFP chimera. Each fusion protein was transiently expressed in HeLa and GHD-1 carcinoma cells, and the endoplasmic reticulum was stained with Texas-red-conjugated wheat germ agglutinin (TR-WGA). Neither AAA-TOB3$_s$-YFP nor AAA-TOB3$_l$-YFP co-lo-

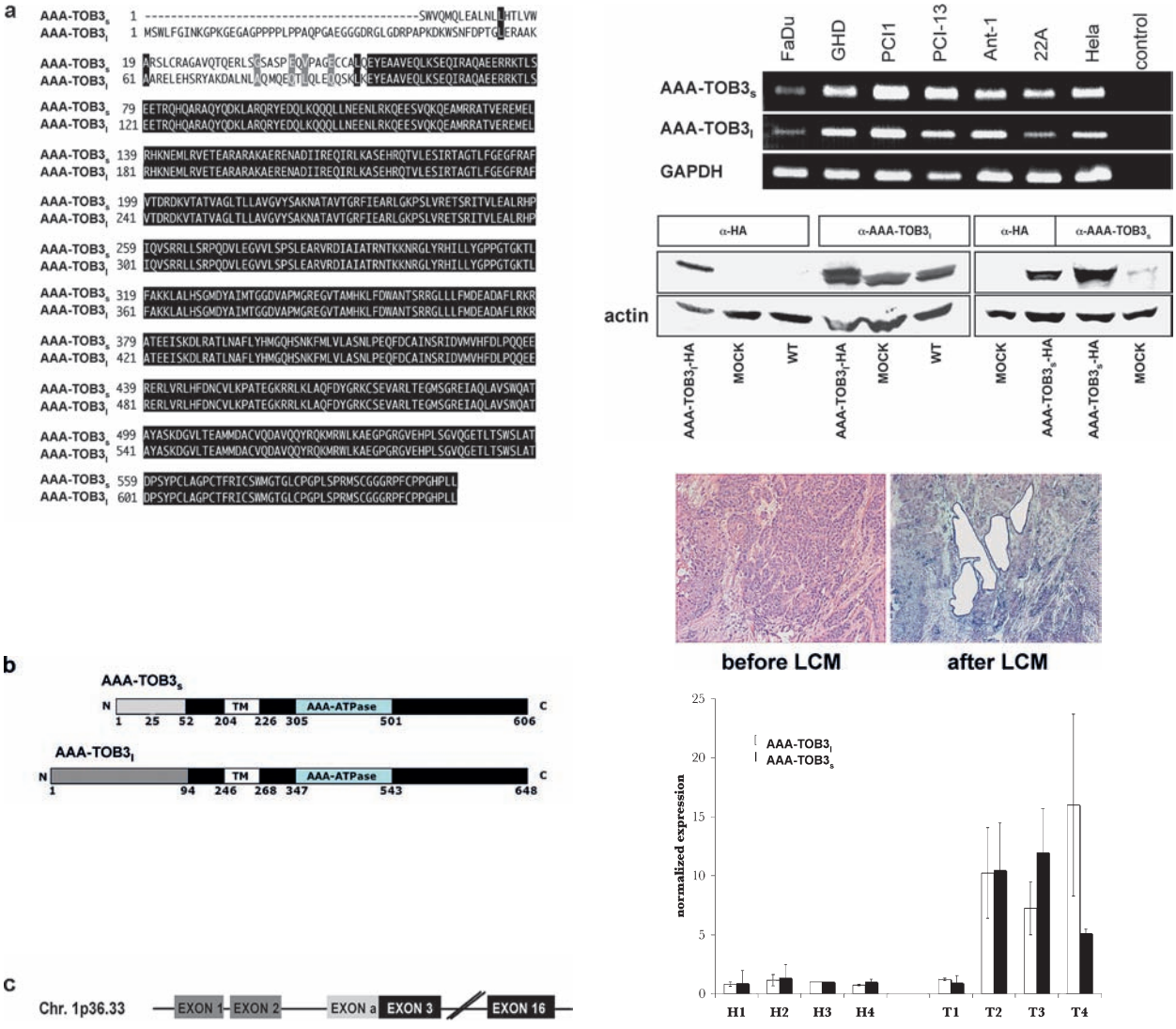

Figure 1. (*a*) Amino acid sequence alignment of the human proteins AAA-TOB3$_s$ and AAA-TOB3$_l$. Identical amino acids are shown in black, similar amino acids in gray. (*b*) Domain architecture of human AAA-TOB3$_s$ and AAA-TOB3$_l$. Both proteins contain an AAA-type ATPase domain in the C-terminal part and a potential transmembrane domain in the N-terminal part. (*c*) Schematic representation of the genomic structure of the human *atad3B* gene. Exon 1 and 2 encode the AAA-TOB3-specific N terminus, exon a encodes the AAA-TOB3$_s$-specific N-terminal part. The common exons 3–16 are shown in black. (*d*) Upper panel: AAA-TOB3$_s$ and AAA-TOB3$_l$ mRNA expression in the cell line HeLa (cervix carcinoma) and in HNSCC cell lines (FaDu, GHD-1, PCI-1, PCI-13, ANT-1, 22A). Control: H_2O. Lower panel: AAA-TOB3$_s$ and AAA-TOB3$_l$ protein expression in the cell line GHD-1. Both, endogenous and HA-tagged fusions were visualized upon immunoblotting with AAA-TOB3$_s$, AAA-TOB3$_l$, and HA-specific antibodies, respectively. For a control, actin levels were assessed in parallel. (*e*) Total RNA was obtained from laser capture microdissected healthy mucosa (H1-4) and head and neck carcinoma cells (T1-4, exemplified in upper panel). Relative expression levels of AAA-TOB3$_s$ and AAA-TOB3$_l$ mRNAs were assessed upon real-time PCR and normalized for actin and GAPDH mRNA levels. Shown are the mean values and standard deviations of two independent experiments.

calized with TR-WGA in HeLa and GHD-1 carcinoma cells (data not shown). In contrast, both proteins strictly co-localized with mitochondria as shown by co-staining with the MitoTracker-Red™ and subsequent laser scanning confocal microscopy analysis (Fig. 3a, b). For a control, YFP expression plasmid was transiently transfected into HeLa cells, and was homogeneously expressed but excluded from mitochondria, strongly suggesting that the addition of the YFP moiety had no influence on TOB3 localization (Fig. 3c). Thus, AAA-TOB3$_s$ and AAA-TOB3$_l$ localize to the mitochondria.

An earlier publication by DaCruz et al. [7] reported the localization of murine AAA-TOB3 to the inner mitochondrial membrane and its pro-apoptotic potential, when transiently transfected into HeLa carcinoma cells. Since these data would suggest a strong detrimental impact of TOB3 overexpression in carcinoma cells, we conducted an in-depth analysis of the pro-apoptotic potential of human AAA-TOB3$_s$ and AAA-TOB3$_l$. HA-tagged variants were separately transfected into HeLa and GHD-1 cells and the correct expression was verified by immunohistochemistry with HA-specific antibodies (Fig. 4a, and data not shown). Transient transfection efficiency in HeLa and GHD-1 cells was controlled previously with a peGFP-C1 expression vector and was 55% and 70% in average, respectively (data not shown). Next, the vitality of both cell lines was assessed in an MTT conversion assay depending on the amount of AAA-TOB3$_s$ or AAA-TOB3$_l$ expression plasmid transfected. All DNA amounts were adjusted to fit the maximal concentrations using empty

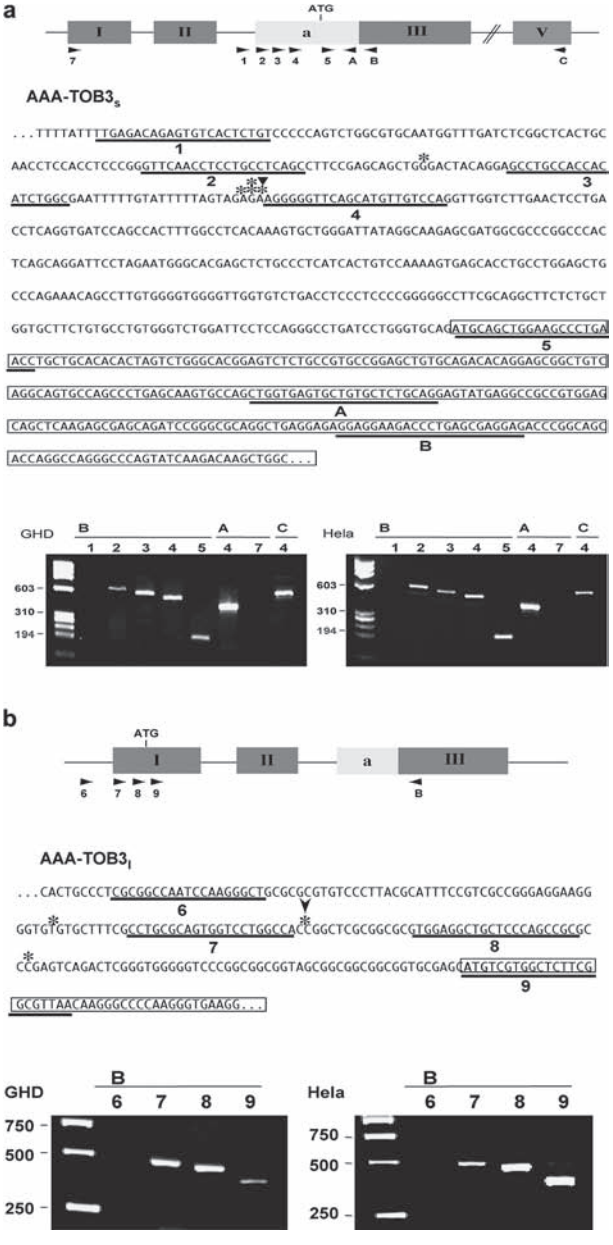

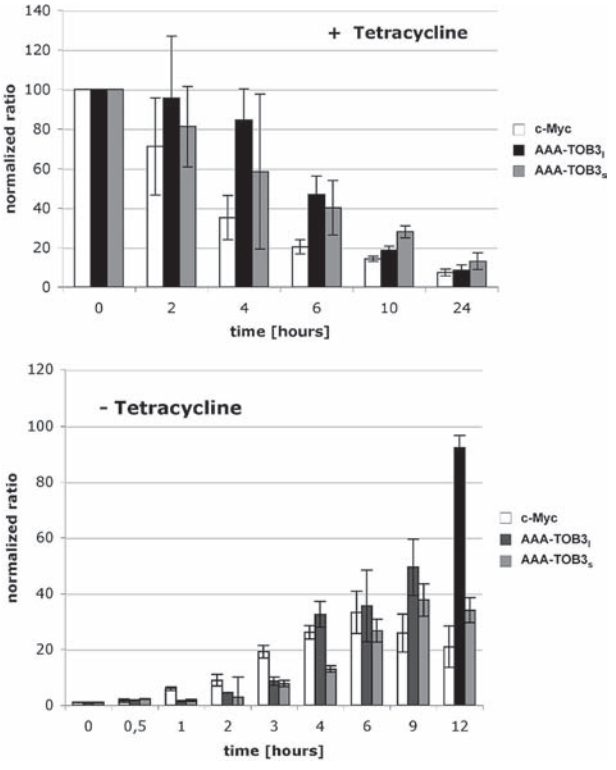

Figure 2. Transcription initiation sites of AAA-TOB3$_s$ (*a*) and AAA-TOB3$_l$ (*b*). Upper panels in (*a*) and (*b*): The transcription start sites as determined by cloning and sequencing of 5′-RACE products are indicated. Asterisks represent the 5′ ends of cloned and sequenced independent products. Lower panels in (*a*) and (*b*): Confirmation of 5′-RACE results by RT-PCR. RT-PCR products obtained with the indicated primer pairs are shown. The binding sites of primers 1–9, and A–C are underlined in the nucleotide sequence in the above schemes. Transcription start sites of human EST clones are marked with arrows. (*c*) C-Myc induced regulation of AAA-TOB3$_s$ and AAA-TOB3$_l$. The expression of c-Myc was repressed (upper panel) and induced (lower panel) in P493-6 B cells by addition or removal of tetracycline. Gene expression of c-Myc, AAA-TOB3$_s$, and AAA-TOB3$_l$ was quantified upon real-time PCR. All values were normalized to CD19 mRNA levels. Shown are the mean and standard deviations of two independent experiments.

vector as a carrier DNA for the specific expression plasmid. Substantial expression of human AAA-TOB3$_s$ or AAA-TOB3$_l$ did not result in any significant reduction in cell vitality, independently of the amount of specific expression plasmid, the time point chosen for the analysis, and the cell line (Fig. 4b, and data not shown).

These findings are in some contrast to the data from DaCruz et al. For this reason, we recapitulated the experiments with transient transfection of YFP fusions of human AAA-TOB3$_s$ and AAA-TOB3$_l$ in HeLa cells, as did DaCruz and colleagues. YFP, AAA-TOB3$_s$-YFP, and AAA-TOB3$_l$-YFP were transiently expressed to similar amounts in HeLa and GHD-1 cells, and the apoptotic index was measured in transfected cells, *i.e.* YFP-positive cells ($100 \leq n \leq 300$), upon annexin-V/PI staining. Due to the strong fluorescence of YFP-tagged variants of TOB3, a parallel measurement of Annexin-V/PI and TOB3-YFP in a standard FACS device was not feasible. In no case did the expression of AAA-TOB3$_l$-YFP or AAA-TOB3$_s$-YFP lead to a specific induction of apoptosis as compared with YFP alone (Fig. 4c). For a control, the pro-apoptotic gene *bax* was transiently transfected at concentrations ranging from 10 ng to 0.5 µg expression plasmid. Expectedly, *bax* induced a marked and concentration-dependent apoptosis in HeLa cells (data not shown). Thus, neither HA- nor YFP-tagged TOB3 variants induced any signs of apoptosis.

To further underscore these findings, both proteins were stably overexpressed as HA-tagged variants in the head and neck carcinoma cell line GHD-1 and detected upon immunoblotting with an HA-specific antibody (see Fig. 1d). Thereafter, the vitality of stable transfectants was assessed in a standard MTT assay over a time period of 4 days in the presence of 1% or 10% FCS. No decrease in cell vitality of AAA-TOB3$_s$ or AAA-TOB3$_l$ transfectants was observable, as compared with vector control GHD-1 transfectants. In contrast, the enforced expression of AAA-TOB3$_l$ resulted in a slight improvement in cell viability under low serum conditions (Fig. 4d).

The effect of the knock-down of AAA-TOB3$_s$ and AAA-TOB3$_l$ protein expression was studied in human carcinoma cells. Specific siRNAs were transiently transferred into GHD-1 cells over a time period of 24–72 h. After 48 h, the expression of AAA-TOB3$_s$ and AAA-TOB3$_l$ was reduced by 53% and 82%, respectively, as assessed by real-time PCR (Fig. 5a). The proliferation of control- and AAA-TOB3$_{s/l}$-siRNA-treated cells was assessed over 4 days. The inhibition of AAA-TOB3$_{s/l}$ expression resulted in a mean 2.4-fold decrease in cell number after 4 days (Fig. 5b). The treatment of GHD-1 cells with control-siRNA had no effect on cell growth, as compared with untreated cells (data not shown). Phenotypically, the knock-down of both proteins led to an increase in cell size and vacuolization of GHD-1 cells. As shown upon flow cytometry, the transfer of AAA-TOB3$_{s/l}$-specific siRNAs into GHD-1 cells resulted in a 3.8-fold increased cell size and 3.5-fold increased granularity as compared with control siRNA-treated cells (Fig. 5c). Notably, cell lines stably carrying expression plasmids for either AAA-TOB3$_s$ or AAA-TOB3$_l$ yielded significantly reduced effects of siRNAs (data not shown). Additionally, ANT-1 cells (HNSCC) and HeLa (cervix) carcinoma cells were treated similarly with AAA-TOB3$_{s/l}$-specific siRNAs. Cell numbers were assessed over 4 days and normalized with values at day 0. ANT-1 and HeLa cells displayed a 2.6-fold and 2.7-fold mean decrease in cell numbers upon treatment with AAA-TOB3$_{s/l}$-specific siRNAs (data not shown). For a control, siRNA transfection efficiency was assessed with FITC-labeled siRNA and was in any case greater than 80%.

The phenotype observed upon treatment with specific siRNA was reminiscent of apoptotic cells. Therefore, we next assessed the apoptotic status of GHD-1 cells de-

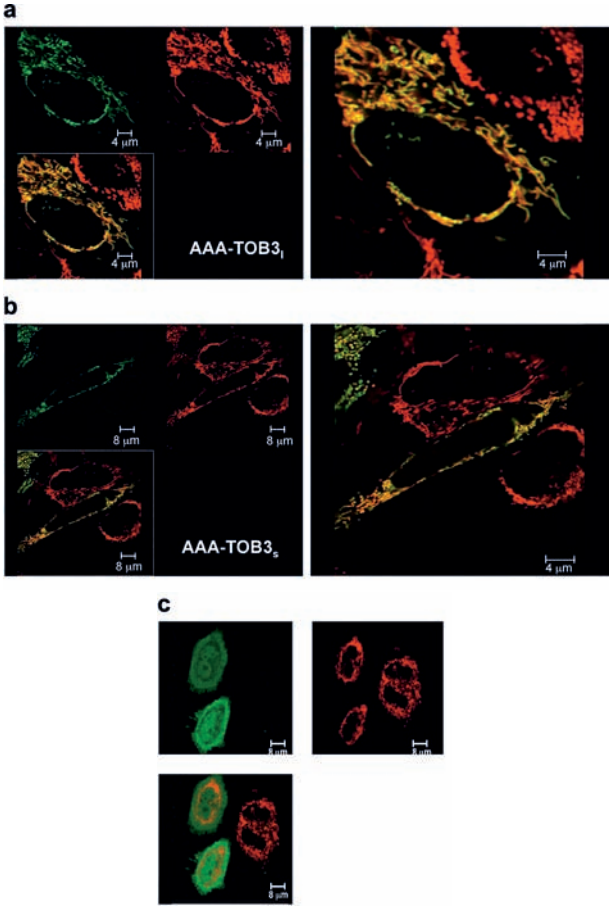

Figure 3. Mitochondrial localization of AAA-TOB3$_s$ (*a*) and AAA-TOB3$_l$ (*b*). C-terminally YFP-tagged human AAA-TOB3$_s$ and AAA-TOB3$_l$ were expressed in HeLa cells. Their subcellular localization was assed by confocal laser scanning microscopy 24 h following transfection. Mitochondria were visualized with Mito-Tracker Red. (*c*) For a control, YFP alone was expressed in HeLa cells and was homogeneously distributed within the cell, except for mitochondria. Shown are representative results from three independent experiments.

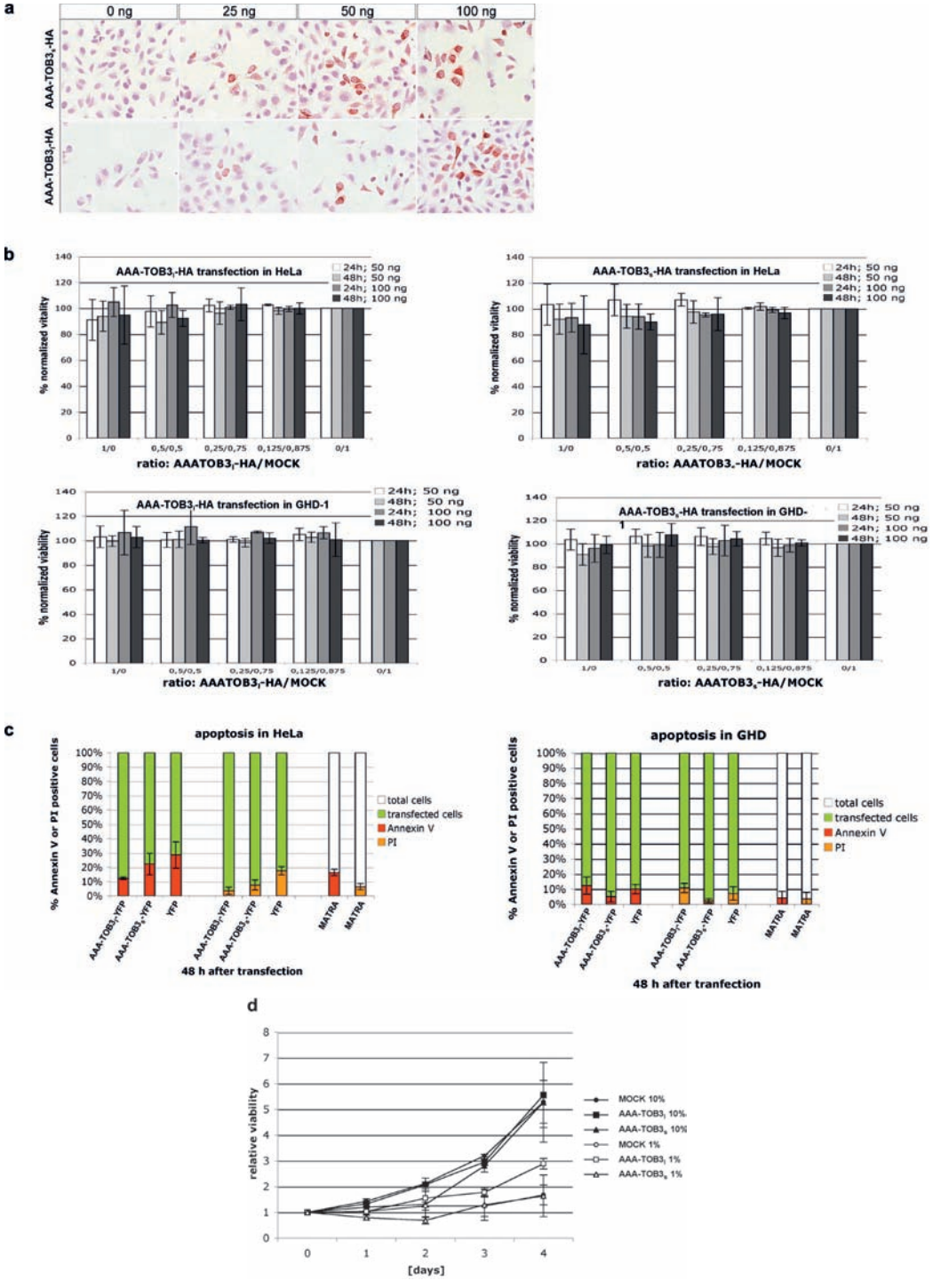

Figure 4. AAA-TOB3$_s$ and AAA-TOB3$_l$ are not pro-apoptotic proteins. (*a*) Increasing amounts of expression plasmids for AAA-TOB3$_s$-HA and AAA-TOB3$_l$-HA were transfected into GHD-1 cells. Visualization of both proteins was performed upon immunohistochemistry and HA-specific antibody (red staining). (*b*) The vitality of HeLa and GHD-1 cells was assessed in a standard MTT assay 24 and 48 h following transient transfection of AAA-TOB3$_s$ (right panel) and AAA-TOB3$_l$ (left panel). Increasing concentrations of expression plasmid were transfected and adjusted to the maximally transfected DNA amount (50 and 100 ng) with empty control vector. Ratios of expression vector and control vector are indicated on the x-axis. Data represent means with standard deviations of three independent experiments. (*c*) HeLa and GHD-1 cells were transiently transfected with the indicated YFP-fusion expression plasmids (100 ng/well). Annexin-V and PI staining was assessed 48 h after transfection. For a control, cells were transfected with an expression plasmid for YFP or treated with transfection reagent only (MATra). Shown are the percentages of annexin-V- or PI-positive cells following treatment with transfection reagent (two rightmost columns) and the percentage of annexin-V- or PI-positive transfected YFP-positive cells (mean ± SD from two independent experiments). (*d*) The indicated stable GHD-1 cell clones were grown in the presence of 1% or 10% FCS over a period of 4 days. Vitality of the cells was assessed using an MTT conversion assay at the indicated time points. Shown are the mean values and standard deviations of three independent experiments.

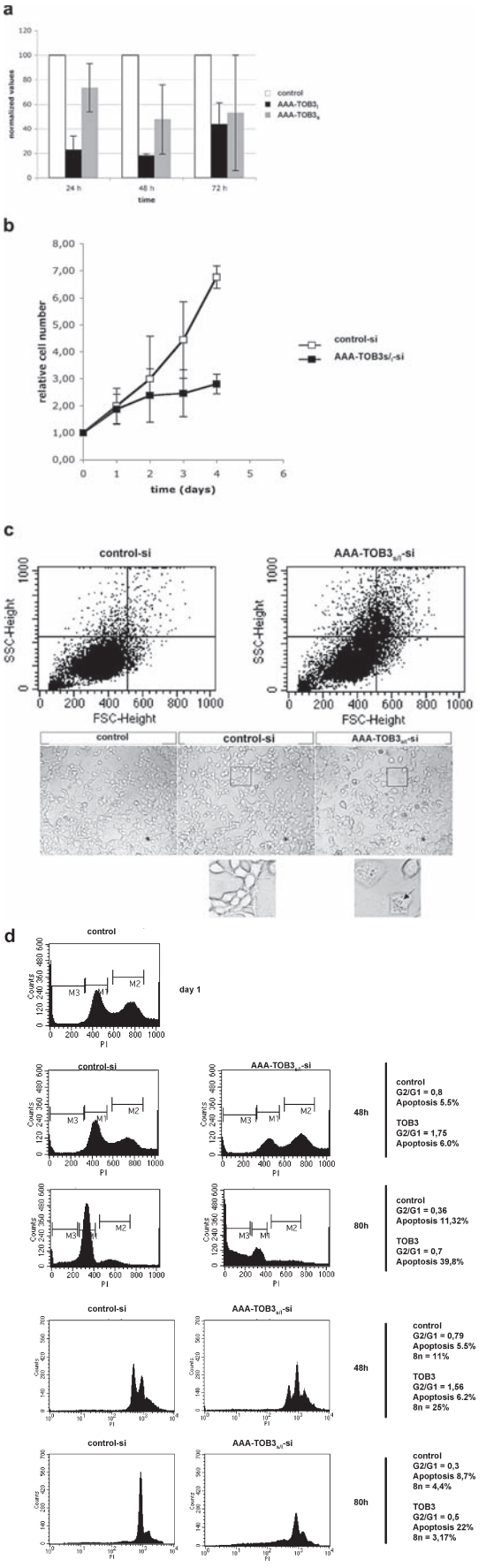

Figure 5. AAA-TOB3$_{s/l}$ knock-down induces apoptosis. (*a*) AAA-TOB3$_s$ and AAA-TOB3$_l$ mRNA expression was assessed upon real-time PCR following treatment of GHD-1 cells with siRNA (100 nM) specific for AAA-TOB3$_s$ and AAA-TOB3$_l$ at the indicated time points. Values were normalized for GAPDH expression and control values (treatment with control-siRNA) set to 100%. Results are mean values and standard deviations from two independent experiments. (*b*) GHD-1 cells were treated with control- or AAA-TOB3$_{s/l}$-siRNA and the cell number assessed over 4 days. All values were normalized to starting cell numbers. Results are mean values and standard deviations from three independent experiments. (*c*) Cell size (FSC) and granularity (SSC) of GHD-1 cells treated with the indicated siRNA molecules were analyzed upon flow cytometry after 68 h and are depicted as a dot plot (upper panel). In parallel, GHD-1 cells transfected with MATra only (control), control-siRNA, or AAA-TOB3$_{s/l}$-siRNA were visualized by light microscopy. (*d*) GHD-1 cells were treated as in (*c*) and sub-G1 DNA fragments analyzed by flow cytometry following intracellular PI staining after 48 and 80 h. M1: G1-phase cells, M2: G2-phase cells, M3: sub-G1 phase cells, M4: polynucleated cells. PI staining was assessed in a linear (upper panels) and logarithmic manner (lower panels). (*e*) GHD-1 cells were treated as in (*c*) and stained for annexin-V and PI. At the time points indicated, the percentage of annexin-V-positive and annexin-V plus PI-positive cells were determined amongst transfected cells. Given are the mean values with standard deviations of three independent experiments. (*f*) GHD-1 cells were treated with control- or AAA-TOB3$_{s/l}$-siRNA and were stained with β-catenin-specific antibody (green) 68 h following treatment. Nuclei were stained with DAPI (blue). Cells were visualized by laser scanning confocal microscopy and are depicted as representative sections. (*g*) Cells were treated as in (*f*) and cells (n = 100) carrying one, two, or more nuclei were counted after 68 h under laser scanning microscopy conditions. The given percentage of each cell population is a mean value of two independent experiments.

pending on the treatment with specific or control siRNA. Starting from day 1 post transfection of siRNA, cells were permeabilized, cellular DNA was stained with PI, and the contents of G1, G2, and sub-G1 DNA were analyzed by flow cytometry. After 68 h, cells treated with specific siRNA displayed an increased amount of cells in the G2/M cell cycle phase (Fig. 5d). After 80 h, a large proportion of these cells contained degraded sub-G1 DNA, which was indicative of apoptotic cells (Fig. 5d). Of note, although cells displayed similar apoptotic values after 48 h, those treated with AAA-TOB3-siRNA yielded 3–4-fold more cells in the subG1 compartment after 80 h. Moreover, the measurement of DNA contents on a logarithmic scale demonstrated the increased presence of cells with higher DNA amounts (*i.e.* 2.5-fold increase in 8n DNA content) after 48 h, thus before onset of apopto-

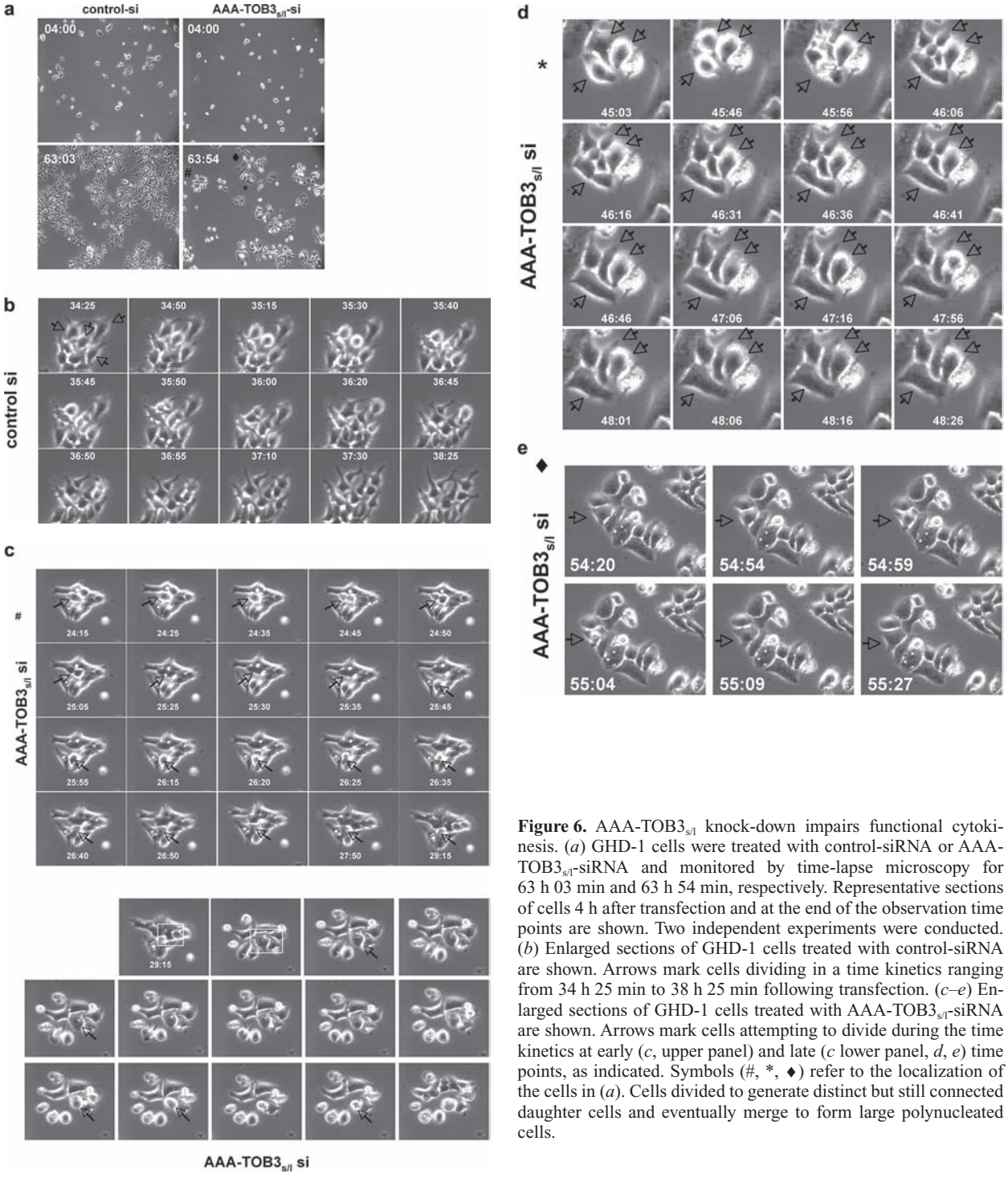

Figure 6. AAA-TOB3$_{s/l}$ knock-down impairs functional cytokinesis. (*a*) GHD-1 cells were treated with control-siRNA or AAA-TOB3$_{s/l}$-siRNA and monitored by time-lapse microscopy for 63 h 03 min and 63 h 54 min, respectively. Representative sections of cells 4 h after transfection and at the end of the observation time points are shown. Two independent experiments were conducted. (*b*) Enlarged sections of GHD-1 cells treated with control-siRNA are shown. Arrows mark cells dividing in a time kinetics ranging from 34 h 25 min to 38 h 25 min following transfection. (*c*–*e*) Enlarged sections of GHD-1 cells treated with AAA-TOB3$_{s/l}$-siRNA are shown. Arrows mark cells attempting to divide during the time kinetics at early (*c*, upper panel) and late (*c* lower panel, *d*, *e*) time points, as indicated. Symbols (#, *, ♦) refer to the localization of the cells in (*a*). Cells divided to generate distinct but still connected daughter cells and eventually merge to form large polynucleated cells.

sis (Fig. 5d). After 80 h, the percentage of cells with an 8n DNA content was back to basal levels, whereas apoptosis was increased by of 2.5-fold (Fig. 5d).

Next, cells were transfected with each siRNA and unpermeabilized cells were stained with FITC-labeled annexin-V and PI over a period of 5 days. The fluorescence of both labels, *i.e.* FITC and PI, was assessed by fluorescence microscopy. At day 3 after transfection, cells treated with specific siRNA showed an increase of annexin-V-positive cells as compared with control-treated cells. This difference increased over time, with 30% and 2.5% annexin-V-positive cells at day 5 in the population treated with specific *versus* control siRNA, respectively (Fig. 5e). The uptake of PI in annexin-V-positive cells started at day 4, thus delayed compared with the annexin-V staining. This is in line with cells undergoing apoptosis, where annexin-V positivity is a hallmark of early apoptosis. At day 5 after treatment, all cells positive for annexin-V also incorporated PI (Fig. 5e).

Using Hoechst 33342 dye for the staining of nuclear DNA, we observed a marked appearance of polynucleated cells in the GHD-1 population treated with AAA-TOB3$_{s/l}$ siRNA, starting at day 2 after transfection (Fig. 5f). This finding was further supported by the appearance of PI peaks with 8n DNA content along with a substantial decrease of G1-phase cells at day 2 (Fig. 5d). Quantification of polynucleated cells at day 3 revealed a severe imbalance, with 20% of cells bearing two nuclei and 40% with more than two nuclei upon AAA-TOB3$_{s/l}$ inhibition in average (Fig. 5g). In a next step, cells were seeded in a living cell chamber and digital photographs were taken every 5 min for 63 h, starting 4 h after transfection, in time-lapse microscopy experiments. For this purpose, cells were either treated with control-siRNA or with the AAA-TOB3$_{s/l}$-specific siRNA. Treatment with AAA-TOB3$_{s/l}$ siRNA led to a markedly diminished cell number, increased yield of round-shaped apoptotic cells, and a substantial proportion of oversized cells amongst the remaining vital cells (Fig. 6a). GHD-1 cells treated with control siRNA divided properly, generating two distinct cells after cytokinesis was fulfilled (Fig. 6b). In contrast, the knock-down of AAA-TOB3$_{s/l}$ in GHD-1 cells resulted in defective cell division in a large proportion of the cells. Over time, cells attempted to divide, showed a clear constriction between dividing daughter cells, but did not manage to terminate cell division. Eventually, intended daughter cells merged to form an enlarged cell (Fig. 6c–e). This failure to fulfill cell division was observable at different periods of time following transfection of specific siRNA. Over time, these defective cells would die (Fig. 6c lower panel, and compare Fig. 6a and c, #-marked cells) or perform further rounds of unfinished cell division, yielding even larger cells, before dying (Fig. 6d, e). Thus, inhibition of AAA-TOB3$_{s/l}$ expression resulted in apoptosis preceded by a failure to divide properly.

Discussion

We have recently described a novel target identification technology designed to isolate potential TAAs, which elicit a humoral response *in vivo* [1]. Amongst the TAAs identified in an autologous screening, several proteins of unknown function appeared to be of special interest, including KIAA1273/AAA-TOB3 [1, 2]. KIAA1273 and AAA-TOB3 have up to now been used as synonyms of the protein product of the *atad3b* gene locus, and the AAA-TOB3 nomenclature is used in the following. AAA-TOB3 was isolated as a cDNA encoding for a large protein expressed in the human brain [12–18]. Expression profiling of the mRNA for AAA-TOB3 demonstrated its weak expression in healthy brain, liver, testis and ovary (http://www.kazusa.or.jp/huge/gfpage/KIAA1273/), which is reminiscent of cancer-testis antigens such as MAGE1 and others [19].

In the present study, we show that the *atad3b* gene locus encodes for two isoforms of AAA-TOB3, which are both overexpressed in squamous cell carcinomas. Both mRNAs are generated upon differential usage of TIS within *atad3b*, and share no homology in the 5′-UTR. The shorter variant initiates transcription at an alternative ATG located within intron 2 of the genomic sequence. Both isoforms entirely differ within the N terminus of the proteins, albeit displaying 95% homology, including the AAA-ATPase and transmembrane domain. Based on the differences in size, the identified isoforms were coined AAA-TOB3$_s$ and AAA-TOB3$_l$, referring to a small and a large variant, respectively. AAA-ATPases can be divided into five sub-groups based on their function and structure [5]. AAA-TOB3$_s$ and AAA-TOB3$_l$ share highest homology with the FtsH and 26S-regulatory subunit proteins (47% and 50% homology, respectively). FtsH are metalloproteases located in the inner mitochondrial membrane, whose substrates are misfolded components of the respiratory complexes [3, 4]. The 26S-proteasome subunits bind proteins, which are targets for degradation and transfer them to peptidases within the 26S-proteasome [6].

In sharp contrast to unpublished data by Pillai et al., suggesting the localization of human AAA-TOB3 in the endoplasmic reticulum, both proteins associated with mitochondria in human carcinoma cells. The cell type studied by Pillai et al., *i.e.* B cells, may account for the observed differences in localization. However, this remains to be assessed experimentally. The murine homolog of AAA-TOB3$_l$, mAAA-TOB3, was identified in a screen for novel proteins of the inner mitochondrial membrane [7]. In line with these findings, we demonstrated the strict co-localization of human AAA-TOB3$_s$ and AAA-TOB3$_l$ with mitochondria. mAAA-TOB3 was shown to have a pro-apoptotic potential when transfected into the human cervix carcinoma cell line HeLa. Since AAA-TOB3$_s$ and

AAA-TOB3$_l$ were both overexpressed in cancer cell lines and in primary carcinomas, we wondered whether the human homologs of mAAA-TOB3 were also pro-apoptotic in nature. This is of interest, as a pro-apoptotic potential was reported for other tumor-associated proteins, such as the cancer-testis antigens MAGE-4A and PRAME [8, 9]. AAA-TOB3$_s$ or AAA-TOB3$_l$ did not induce cell death under any circumstances in two distinct human carcinoma cell lines, *i.e.* HeLa and GHD-1. This clear functional discrepancy can have several reasons: (i) mAAA-TOB3 and hAAA-TOB3$_{s/l}$ may have opposing functions despite their high homology of 72%, (ii) mAAA-TOB3 may induce apoptosis in a xenogenic system, *i.e.* in human cells. This assumption is suggested by the fact that six out of seven murine mitochondrial proteins induced apoptosis when transfected into HeLa cells. However, it is intriguing that the single protein, which did not induce apoptosis significantly, lacked a transmembrane domain. Thus, it cannot be excluded that the overexpression of mouse proteins, which insert in the membrane of mitochondria, induced apoptosis rather unspecifically, due to changes in the mitochondrial membrane potential or membrane disruption. (iii) A third point adding to the observed discrepancy might also be the amount of DNA used for the respective transfection experiments. In the present study, all DNA amounts were standardized upon addition of carrier-DNA since increasing amounts of transfected DNA resulted in substantially decreased vitality of HeLa cells (data not shown).

These findings were further substantiated by the fact that the inhibition of both AAA-TOB3$_s$ and AAA-TOB3$_l$ using siRNAs resulted in apoptosis associated with decreased proliferation, enlargement of cells, vacuolization, and the generation of polynucleated cells. The assessment of DNA content together with time-lapse microscopy demonstrated that inhibition of AAA-TOB3$_{s/l}$ resulted in dysfunctions in the process of cell division and eventually cell death by apoptosis. These processes were obviously interdependent and coordinated in time, producing a dysfunctional cell division preceding apoptosis. GHD-1 cells treated with AAA-TOB3$_{s/l}$-specific siRNA attempted to fulfill the cell cycle and terminate mitotic division. Recently, Castedo et al. [20] reported on tetraploid cells with a decreased sensitivity towards DNA damaging agents and UV irradiation. Nonetheless, these cells which failed to terminate cytokinesis are dictated to undergo Bax-dependent apoptosis. In our case, to-be daughter cells did not manage to divide properly, remained adjunctive and eventually merged to generate large, polynucleated cells, followed by their cell death. In full accordance with the suggested role in cell division, AAA-TOB3 was reported to be a substrate for Aurora B kinase, a major regulator of mitotic checkpoints and cell division [21]. Two additional carcinoma cell lines, *i.e.* HeLa and ANT-1 comparably responded to the knock-down of AAA-TOB3$_{s/l}$ with a decreased cell number. However, HeLa cells did not yield polynucleated cells, but rather induced rapidly apoptosis upon siRNA treatment. This may reflect differences in genes involved in the check-points controlling progression of mitotic cells [22–27]. Mutations in check-points of mitotic division may allow GHD-1 and ANT-1 cells to progress through cell cycle despite incorrect cytokinesis, resulting in polynucleated cells.

In summary, we demonstrate here for the first time, that AAA-TOB3$_s$ and AAA-TOB3$_l$ are two distinct proteins generated from the *atad3b* gene locus under the control of the oncogenic factor c-Myc. The inhibition of both transcripts using siRNAs resulted in incorrect cell division and thereafter apoptosis, thus strongly suggesting a role in proper cytokinesis.

Acknowledgements. Part of the work was supported by grants of the Else-Kröner-Fresenius-Stiftung and the Deutsche Forschungsgemeinschaft (GI540/1-1) to O.G and C.M. We thank Jens Rauch and Dr. Markus Münz for helpful discussions and critical reading of the manuscript. We thank Prof. Eisenmenger, Dr. Anslinger, and Mrs. Bayer for their help with laser capture microdissection experiments. Intellectual property of the AMIDA technology resides at Vaecgene Biotec. The authors have no conflicting financial interest.

1 Gires, O., Munz, M., Schaffrik, M., Kieu, C., Rauch, J., Ahlemann, M., Eberle, D., Mack, B., Wollenberg, B., Lang, S., Hofmann, T., Hammerschmidt, W. and Zeidler, R. (2004) Profile identification of disease-associated humoral antigens using AMIDA, a novel proteomics-based technology. Cell. Mol. Life Sci. 61, 1198–1207.
2 Rauch, J., Ahlemann, M., Schaffrik, M., Mack, B., Ertongur, S., Andratschke, M., Zeidler, R., Lang, S. and Gires, O. (2004) Allogenic antibody-mediated identification of head and neck cancer antigens. Biochem. Biophys. Res. Commun. 323, 156–162.
3 Langer, T., Kaser, M., Klanner, C. and Leonhard, K. (2001) AAA proteases of mitochondria: quality control of membrane proteins and regulatory functions during mitochondrial biogenesis. Biochem. Soc. Trans. 29, 431–436.
4 Karata, K., Verma, C. S., Wilkinson, A. J. and Ogura, T. (2001) Probing the mechanism of ATP hydrolysis and substrate translocation in the AAA protease FtsH by modelling and mutagenesis. Mol. Microbiol. 39, 890–903.
5 Lupas, A. N. and Martin, J. (2002) AAA proteins. Curr. Opin. Struct. Biol. 12, 746–753.
6 Ogura, T. and Wilkinson, A. J. (2001) AAA+ superfamily ATPases: common structure – diverse function. Genes Cells 6, 575–597.
7 Da Cruz, S., Xenarios, I., Langridge, J., Vilbois, F., Parone, P. A. and Martinou, J. C. (2003) Proteomic analysis of the mouse liver mitochondrial inner membrane. J. Biol. Chem. 278, 41566–41571.
8 Sakurai, T., Itoh, K., Higashitsuji, H., Nagao, T., Nonoguchi, K., Chiba, T. and Fujita, J. (2004) A cleaved form of MAGE-A4 binds to Miz-1 and induces apoptosis in human cells. J. Biol. Chem. 279, 15505–15514.
9 Tajeddine, N., Gala, J. L., Louis, M., Van Schoor, M., Tombal, B. and Gailly, P. (2005) Tumor-associated antigen preferentially expressed antigen of melanoma (PRAME) induces caspase-independent cell death *in vitro* and reduces tumorigenicity *in vivo*. Cancer Res. 65, 7348–7355.
10 Mayer, A., Andratschke, M., Pauli, C., Graefe, H., Kristina, K. and Wollenberg, B. (2005) Generation of an autologous cell system for immunotherapy of squamous cell carcinoma of the head and neck. Antiancer Res. 25, 4075–4080.

11 Schuhmacher, M., Kohlhuber, F., Holzel, M., Kaiser, C., Burtscher, H., Jarsch, M., Bornkamm, G. W., Laux, G., Polack, A., Weidle, U. H. and Eick, D. (2001) The transcriptional program of a human B cell line in response to Myc. Nucleic Acids Res. 29, 397–406.
12 Kikuno, R., Nagase, T., Nakayama, M., Koga, H., Okazaki, N., Nakajima, D. and Ohara, O. (2004) HUGE: a database for human KIAA proteins, a 2004 update integrating HUGEppi and ROUGE. Nucleic Acids Res. 32, D502–504.
13 Nagase, T., Kikuno, R., Ishikawa, K., Hirosawa, M. and Ohara, O. (2000) Prediction of the coding sequences of unidentified human genes. XVII. The complete sequences of 100 new cDNA clones from brain which code for large proteins *in vitro*. DNA Res. 7, 143–150.
14 Nagase, T., Kikuno, R., Ishikawa, K. I., Hirosawa, M. and Ohara, O. (2000) Prediction of the coding sequences of unidentified human genes. XVI. The complete sequences of 150 new cDNA clones from brain which code for large proteins *in vitro*. DNA Res. 7, 65–73.
15 Nagase, T., Kikuno, R., Nakayama, M., Hirosawa, M. and Ohara, O. (2000) Prediction of the coding sequences of unidentified human genes. XVIII. The complete sequences of 100 new cDNA clones from brain which code for large proteins *in vitro*. DNA Res. 7, 273–281.
16 Nagase, T., Kikuno, R. and Ohara, O. (2001) Prediction of the coding sequences of unidentified human genes. XXII. The complete sequences of 50 new cDNA clones which code for large proteins. DNA Res. 8, 319–327.
17 Nagase, T., Kikuno, R. and Ohara, O. (2001) Prediction of the coding sequences of unidentified human genes. XXI. The complete sequences of 60 new cDNA clones from brain which code for large proteins. DNA Res. 8, 179–187.
18 Nagase, T., Nakayama, M., Nakajima, D., Kikuno, R. and Ohara, O. (2001) Prediction of the coding sequences of unidentified human genes. XX. The complete sequences of 100 new cDNA clones from brain which code for large proteins *in vitro*. DNA Res. 8, 85–95.
19 Scanlan, M. J., Simpson, A. J. and Old, L. J. (2004) The cancer/testis genes: review, standardization, and commentary. Cancer Immun. 4, 1.
20 Castedo, M., Coquelle, A., Vivet, S., Vitale, I., Kauffmann, A., Dessen, P., Pequignot, M. O., Casares, N., Valent, A., Mouhamad, S., Schmitt, E., Modjtahedi, N., Vainchenker, W., Zitvogel, L., Lazar, V., Garrido, C. and Kroemer, G. (2006) Apoptosis regulation in tetraploid cancer cells. EMBO J. 7, 2584–2595.
21 Morrison, C., Henzing, A. J., Jensen, O. N., Osheroff, N., Dodson, H., Kandels-Lewis, S. E., Adams, R. R. and Earnshaw, W. C. (2002) Proteomic analysis of human metaphase chromosomes reveals topoisomerase II alpha as an Aurora B substrate. Nucleic Acids Res. 30, 5318–5327.
22 Crane, R., Gadea, B., Littlepage, L., Wu, H. and Ruderman, J. V. (2004) Aurora A, meiosis and mitosis. Biol. Cell 96, 215–229.
23 Dai, W., Huang, X. and Ruan, Q. (2003) Polo-like kinases in cell cycle checkpoint control. Front. Biosci. 8, d1128–1133.
24 Dash, B. C. and El-Deiry, W. S. (2004) Cell cycle checkpoint control mechanisms that can be disrupted in cancer. Methods Mol. Biol. 280, 99–161.
25 Meraldi, P., Honda, R. and Nigg, E. A. (2004) Aurora kinases link chromosome segregation and cell division to cancer susceptibility. Curr. Opin. Genet. Dev. 14, 29–36.
26 Tan, A. L., Rida, P. C. and Surana, U. (2005) Essential tension and constructive destruction: the spindle checkpoint and its regulatory links with mitotic exit. Biochem. J. 386, 1–13.
27 van Vugt, M. A. and Medema, R. H. (2005) Getting in and out of mitosis with Polo-like kinase-1. Oncogene 24, 2844–2859.